Photocatalytic CO_2 reduction enhanced by thermochromic effect of modified VO_2

Longzhen Zhang,[a] Yimin Xuan,[a,*] Qi Wang,[a] Zhonghui Zhu,[a] Dawei Zhao,[a] Xianglei Liu,[a] Qibin Zhu,[a] Kai Zhang[a]

[a] School of Energy and Power Engineering, Nanjing University of Aeronautics and Astronautics, Nanjing 210016, China

Content

Experimental section

The preparation of IV catalysts

IV is synthesized by hydrothermal method. In specific method, 1 mmol ammonium met vanadate, 1 mmol indium nitrate were added into 20 mL deionized water, and 0.5 mmol citric acid were added into 10 mL deionized water. Then mix the two solutions and ultrasound dispersed evenly. And then the mixed solution was transferred into a 50 mL Teflon-lined stainless-steel autoclave and heated at180 °C for 3 h. After cooling down, the sample was obtained by filtering, and heated at 40 °C for 12 h.

The preparation of VO_2 and Me_xV Co-catalysts (Me=Mo, Co, W, x=0.05, 0.1)

VO_2 is synthesized by hydrothermal method. In typical method, 2 mmol ammonium met vanadate and 0.5 mmol citric acid were added into 30 mL deionized water, and dispersed by ultra phonic method for 30 minutes evenly. And it was transferred into a 50 mL Teflon-lined stainless-steel autoclave and heated at 160 °C for 12 h. After cooling down, the sample was washed using water by centrifuged and filtered for four times. Finally, heat and dry the sample at 40 °C for 24 h. Similarly, Me_xV is synthesized by hydrothermal method like the procedure of the preparation of VO_2. Specifically, 2 mmol ammonium met vanadate, 0.5 mmol citric acid were added into 20 mL deionized water, and 0.2 or 0.4 mmol molybdenum nitrate or cobalt nitrate or tungstic acid was added into 10 mL deionized water. Then mix the two solutions and dispersed by ultra phonic method for 30 minutes evenly. And it was transferred into a 50 mL Teflon-lined stainless-steel autoclave and heated at160 °C for 12 h. After cooling down, the sample was washed using water by centrifuged and filtered for four times. Finally, heat and dry the sample at 40 °C for 24 h. Then $Mo_{0.05}VO_2$(M1V), $Mo_{0.1}VO_2$ (M2V), $Co_{0.05}VO_2$ (C1V), $Co_{0.1}VO_2$ (C2V), $W_{0.05}VO_2$ (W1V) and $W_{0.1}VO_2$ (W2V) were obtained.

Synthesis of VO_2-IV and Me_xV-IV Composites

100 mg IV and 10 mg Me_xV were mixed into 20 mL H_2O and it was dispersed by ultra phonic method for 1 h. Then the samples were obtained by centrifuged at 10000 r/min for 5 minutes. Then heat, dry the samples at 40 °C for 24 h and grind them. Finally, VO_2-IV, M1V-IV, M2V-IV, C1V-IV, C2V-IV, W1V-IV and W2V-IV were obtained.

Characterizations

The crystallographic phase of these as-prepared powder samples was determined investigated by an in-situ temperature-dependent and ex-situ X-ray diffractometer (XRD; Rigaku Ultima III, Japan) at different temperatures. The rate of rising temperature is 10 °C/min and maintain the test temperature 5 min. The XRD graphs were described over the scanning range of 5°-80° using Cu-Ka radiation (λ = 0.154178 nm) at 40 kV and 40 mA.

The morphologies of the materials and EDS mapping were determined by a field-emission scanning electron microscope (FESEM) by using an accelerating voltage of 5 kV. Transmission electron microscopic (TEM) images were obtained at 200 kV by a transmission electron microscope.

The X-ray photoelectron spectroscopy (XPS) was performed using a spectrometer (Escalab 250xi, Thermo Scientific). The specific surface area and pore size distribution of materials was performed by a physical absorption analyzer.

The UV-vis diffuse reflectance spectra (DRS) of all as-prepared powder samples were recorded using a Perkin Elmer Lambda spectrophotometer and using $BaSO_4$ as standard under different temperatures.

The atomic force microscopic (AFM) images and ex situ and in situ Kelvin probe force

microscope (KPFM) images were performed by an atomic force microscope (NX-Hivac, Park). The KPFM images were displayed in dark or under a LED lamp.
The photoluminescence (PL) spectra of the samples were recorded with a PE LS 55 spectro fluoro photometer. The average carrier lifetime (τ_{ave}) is calculated through the following equation:

$$\tau_{ave} = \frac{A_1{\tau_1}^2 + A_2{\tau_2}^2}{A_1\tau_1 + A_2\tau_2}$$

In situ DRIFT was measured by Nicolet iS50 FTIR (Thermo Scientific) in dark or under a 300 W Xe lamp at a distance of 30 cm. The rate of raising temperature is 10 °C/min and maintain the test temperature 5 min using cooling water when measured. The temperature rise curves of each sample were measured in a closed reactor about 0.5 cm X 0.5 cm without water using a data-recording thermocouple.

Photocatalytic activities for CO_2 conversion

0.02 g of the photocatalyst with glass fiber filter and 2 mL deionized water was placed in a 50 mL quartz reactor. Besides, a 300 W xenon arc lamp was used as reactive light source. Simulated solar spectrogram is displayed in **Figure S27**. Firstly, high-purity (99.999 %) CO_2 with a steady flow was continuously bubbled in the closed reactor to ensure no O_2 and N_2 in the reactor and the CO_2/H_2O adsorption-desorption equilibrium on the photocatalyst for at least 1 h, and then start the light reaction. After irradiation for 6 h, 1 mL mixed gas of the photo-reactor was injected into a gas chromatograph (GC-9720, containing both TCD and FID detectors) to obtain CO and CH_4 concentrations. Meanwhile, control experiments were also done in Ar atmosphere, no light or no catalyst. Furthermore, the reduction products of $^{13}CO_2$ isotope labelling instead of $^{12}CO_2$ experiment were experimented. After light irradiation for two days, 1 mL of the product gas was analyzed by gas chromatography-mass spectrometer (Agilent 7890B 5977B GC-MSD).

Photoelectrochemical measurements

The photoelectrochemical measurements were measured in a three-electrode configuration system (FTO-working electrode, Pt-counter electrode, Ag/AgCl-reference electrode and 0.5 M Na_2SO_4 solution-the electrolyte) on a CHI 760A electrochemical workstation. The photocurrent data were obtained by using a 300 W Xe lamp with filters to with on-off time intervals of 10 s. The linear sweep voltammetry (LSV) was obtained at a scan rate of 50 mV/s in dark or under light. Mott-Schottky curves were tested under the condition at the frequency of 1000 Hz and the scan rate of 50 mV of various potentials in dark.

Theoretical calculation methods

All calculations are performed within the DFT framework using the generalized gradient approximation (GGA) of Perdew-Burke-Ernzerhof (PBE).[1] The VASP (Vienna Ab initio Simulation Package) package and the projection-enhanced wave method are used.[2,3] The kinetic cutoff energy of the planar wave base is set to 600 eV. Brillouin zone integration is performed on a Gamma-centered K-Mesh. The self-consistent field (SCF) procedure is performed with a convergence criterion of 10-8 eV until all atoms are fully relaxed until the force on each atom is less than 0.02 eV/Å. The rutile phase has 72 atoms in 2*2*3 expansion, and the M phase has 48 atoms in 2*2*1 expansion. The (110) and (011) planes of the rutile phase and the m phase were respectively selected for adsorption calculation. The adsorption model consists of 4 layers, the bottom two layers are fixed for calculation, and the vacuum layer is set at 15 angstrom. The energy band structure was calculated by CASTEP.

Supplementary Figure

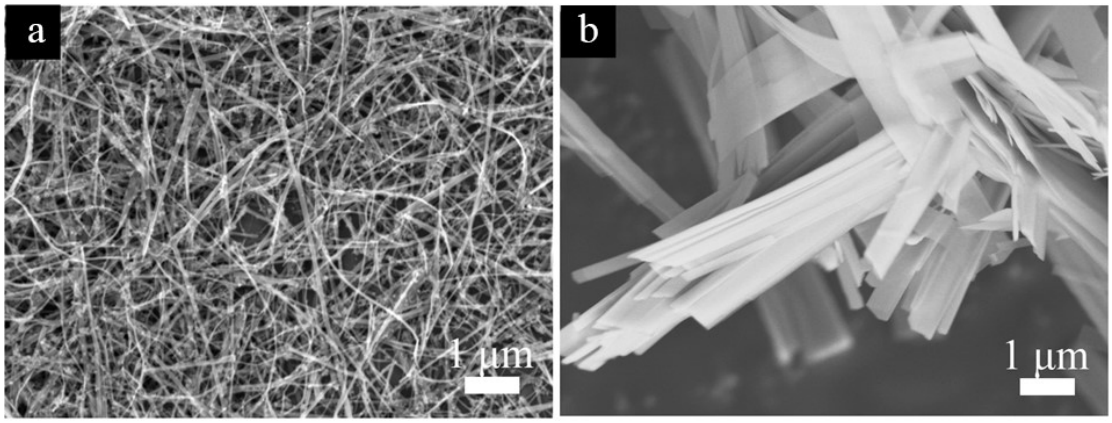

Figure S1. Representative SEM image of synthesized IV and VO_2 material.

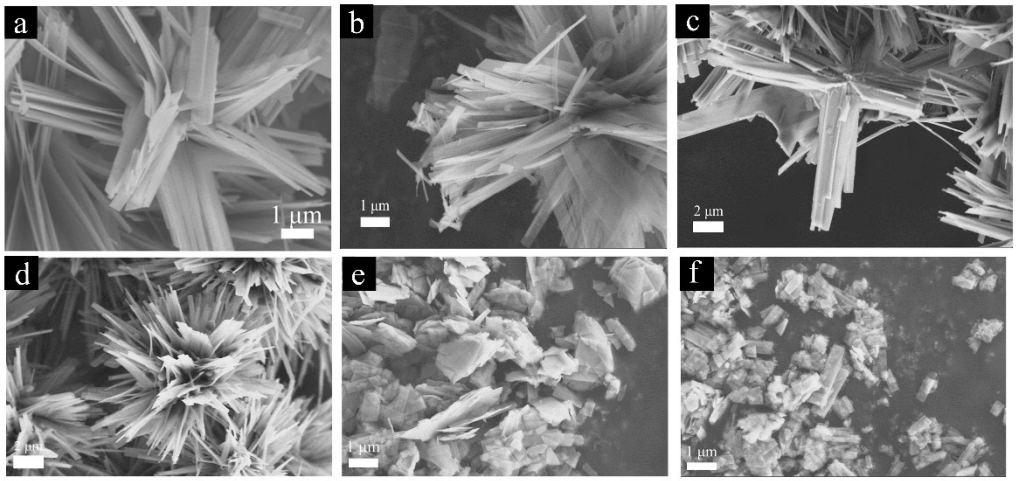

Figure S2 Representative SEM images of synthesized (a) M1V, (b) M2V, (c) C1V, (d) C2V, (e) W1V and (f) W2V.

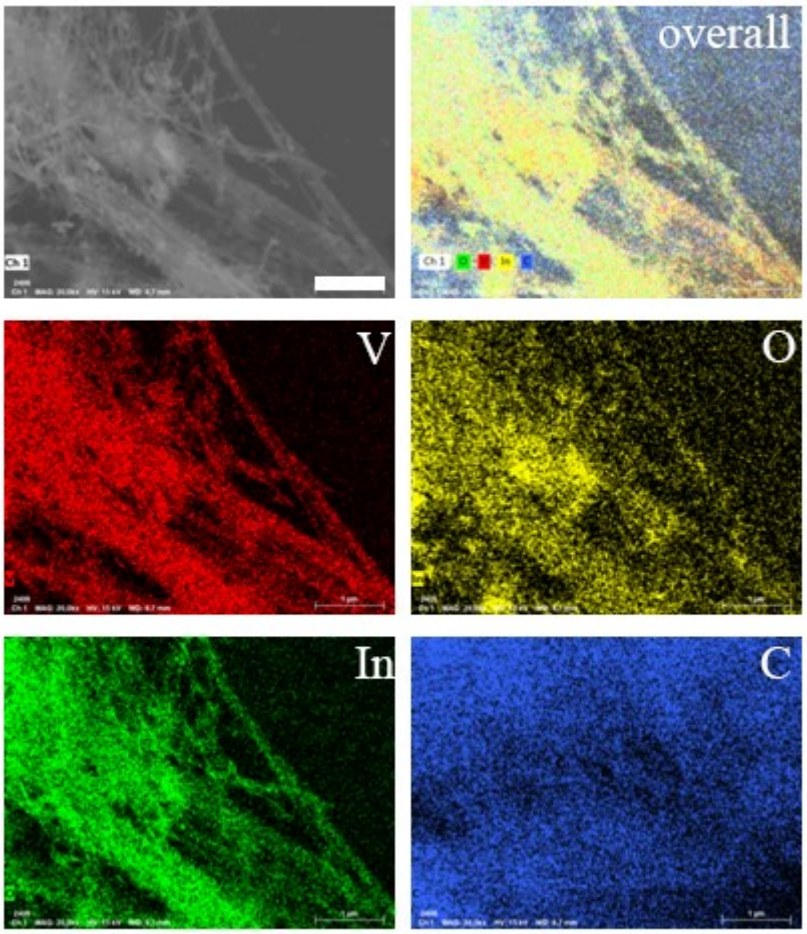

Figure S3 EDS elemental mapping profiles of IV with In (bright yellow), V (red), O (green) and C(blue) distribution.

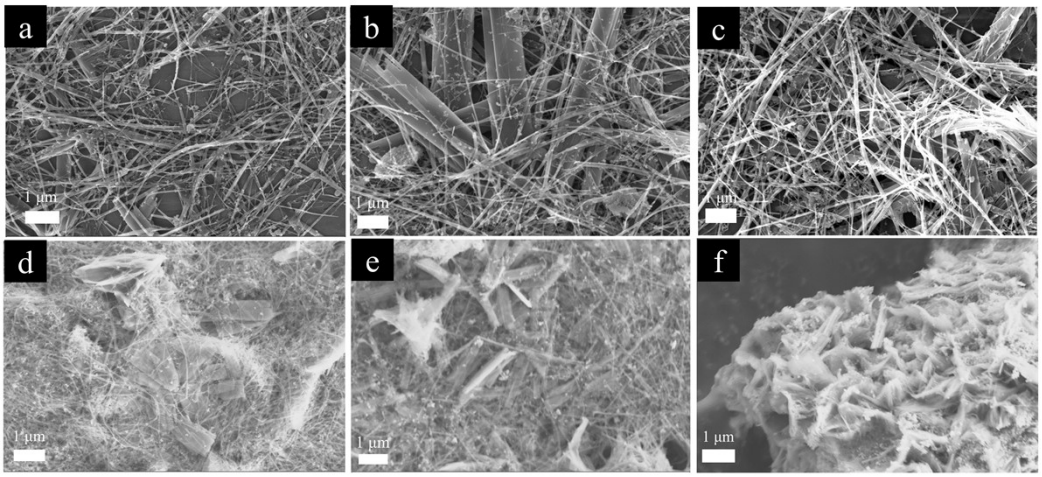

Figure S4 Representative SEM images of synthesized (a) M2V-IV, (b) C1V-IV, (c) C2V-IV, (d) W1V-IV, (e) W2V-IV and (f) VO_2-IV.

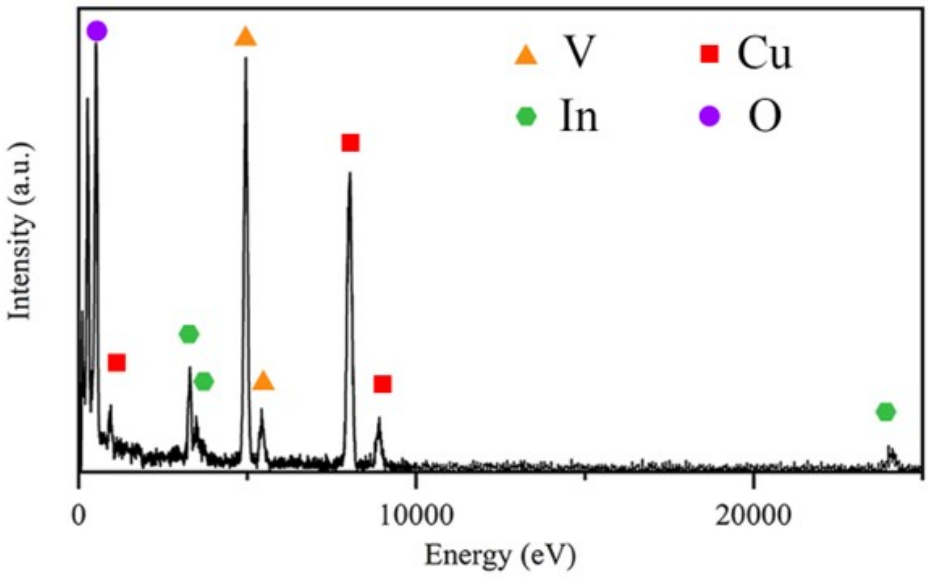

Figure S5 TEM-EDS spectrum of M1V-IV material.

a b

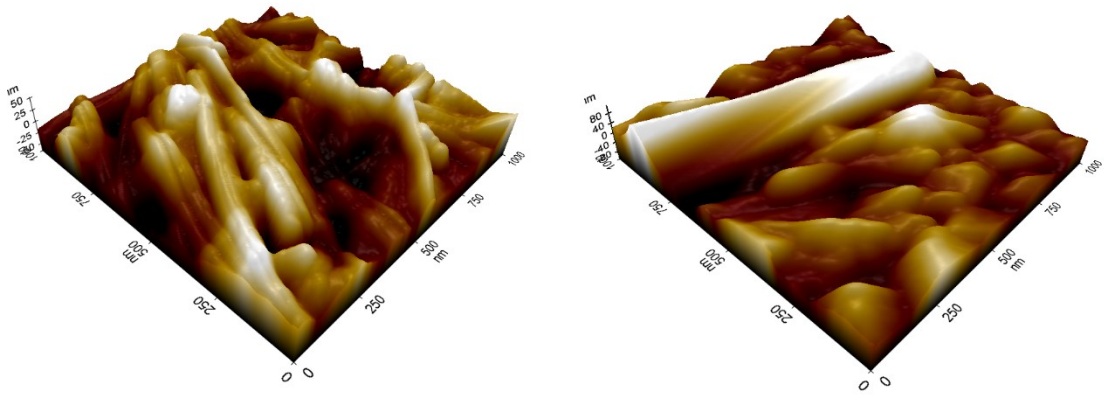

Figure S6 Representative AFM 3D image of IV and M1V.

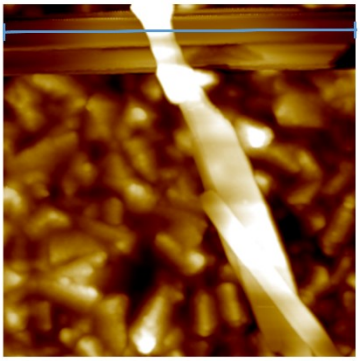

Figure S7 Representative AFM image of VO_2.

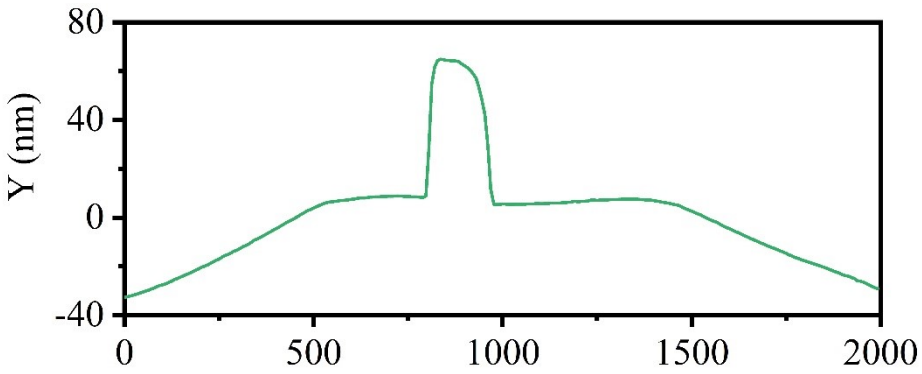

Figure S8 AFM line scanning of VO_2.

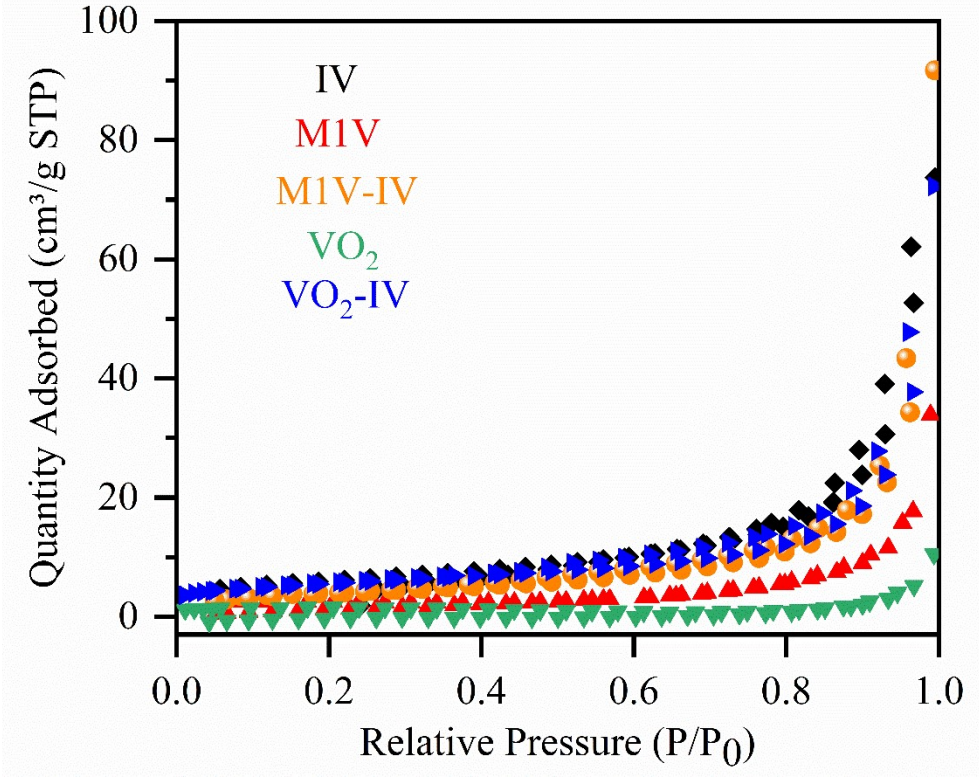

Figure S9 N_2 absorption-desorption isotherms of samples.

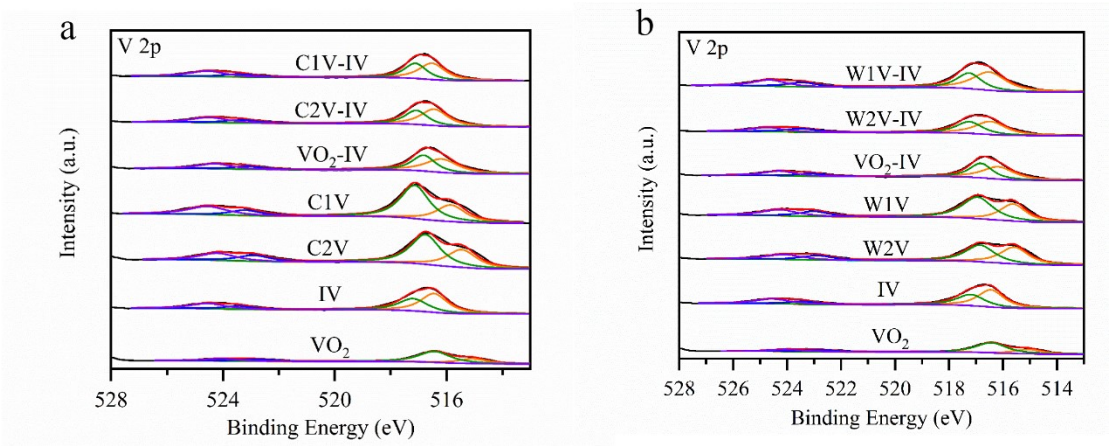

Figure S10 High-resolution XPS spectra of V 2p in C_xV, C_xV-IV, W_xV and W_xV-IV materials.

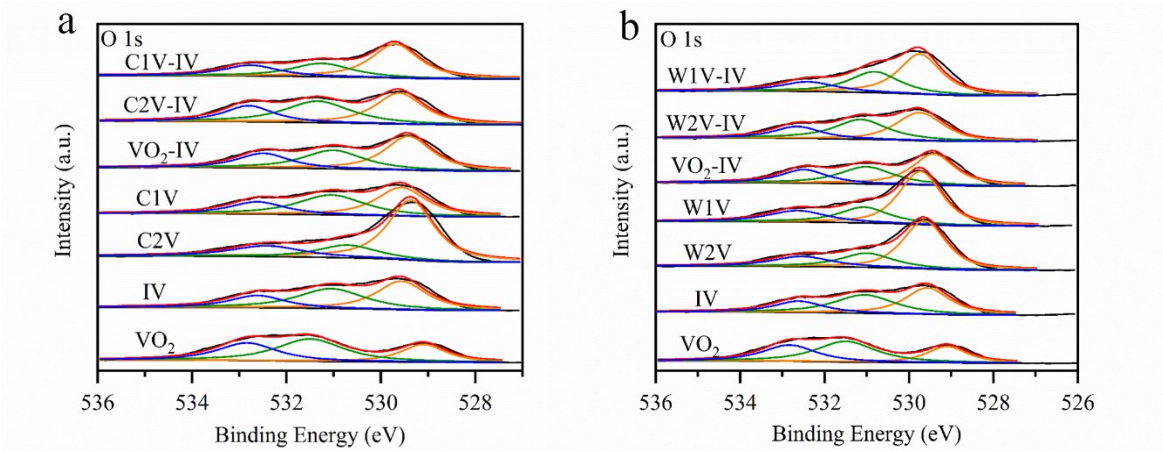

Figure S11 High-resolution XPS spectra of O 1s in C_xV, C_xV-IV, W_xV and W_xV-IV materials.

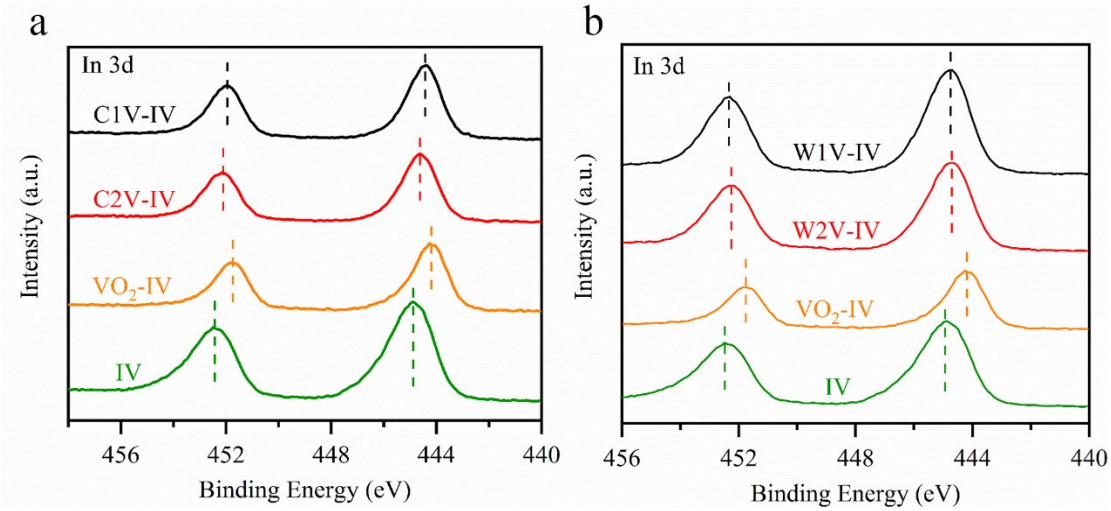

Figure S12 High-resolution XPS spectra of In 3d in C_xV, C_xV-IV, W_xV and W_xV-IV materials.

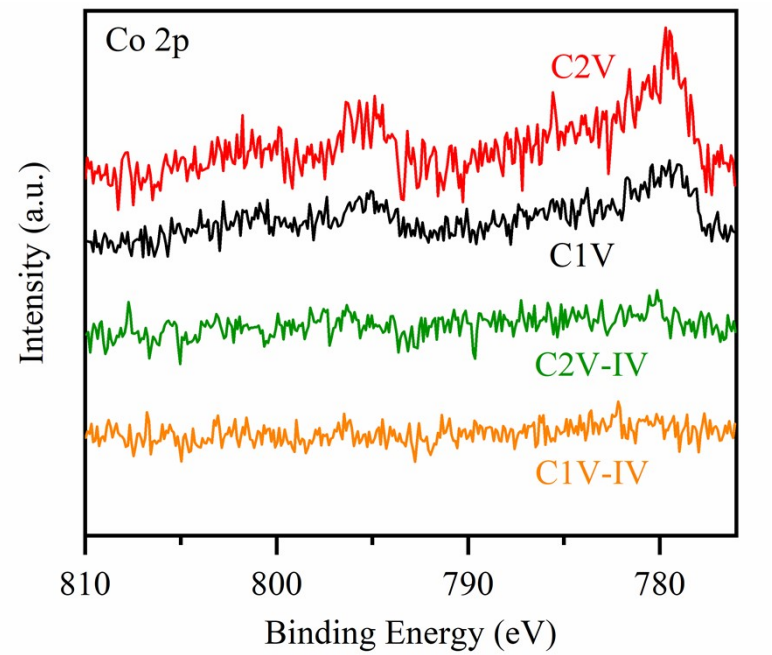

Figure S13 High-resolution XPS spectra of Co 2p in C_xV and C_xV-IV materials.

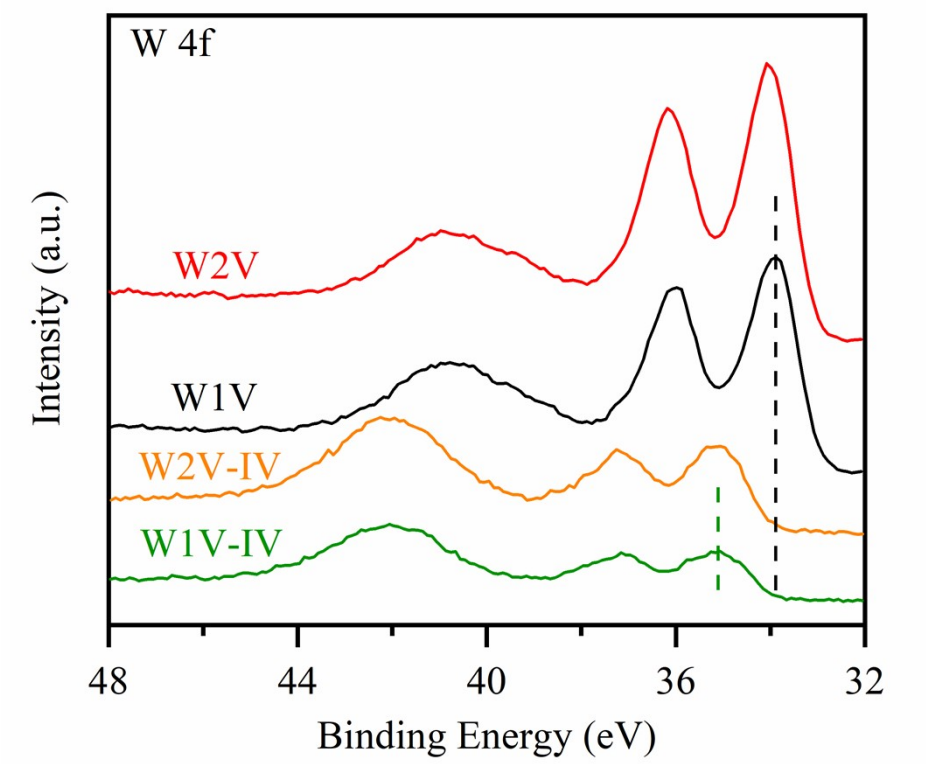

Figure S14 High-resolution XPS spectra of W 4f in W_xV and W_xV-IV materials.

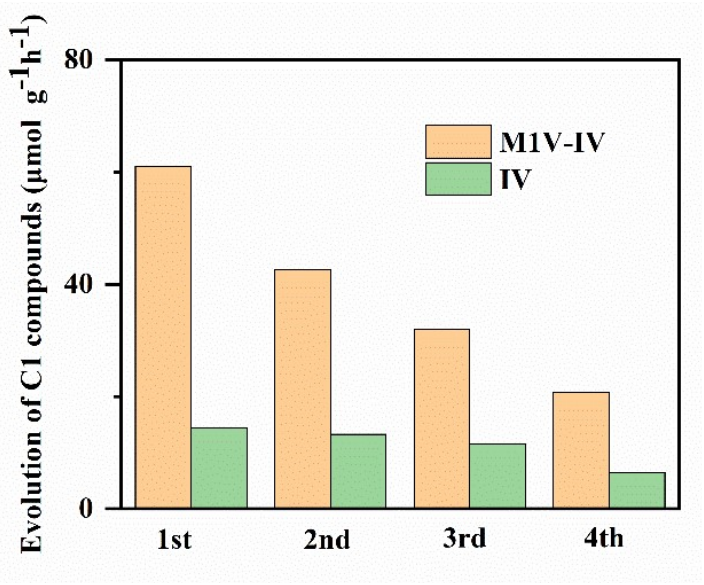

Figure 15 The stability performance of M1V-IV and IV.

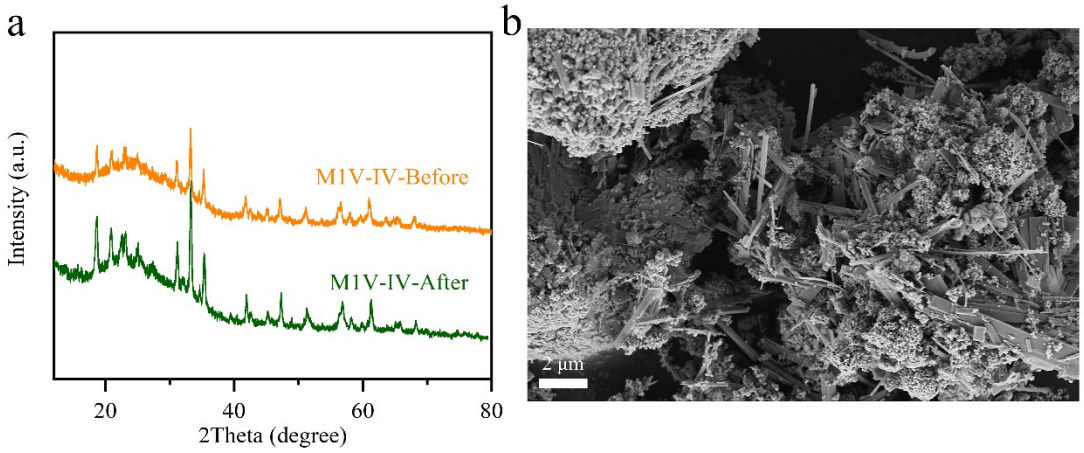

Figure S16 XRD pattern and SEM image of reclaimed M1V-IV.

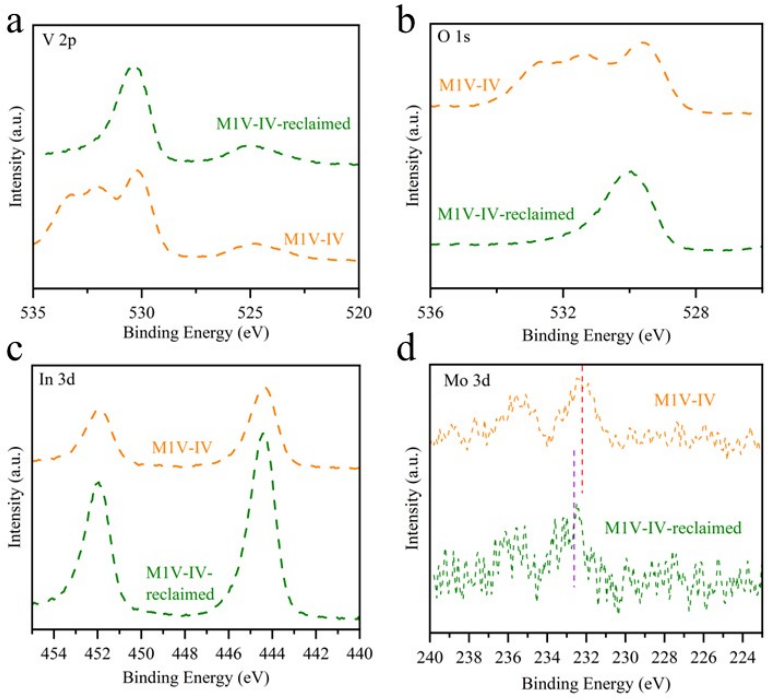

Figure 17 The high-resolution spectra of (a) V 2p, (b) O 1s, (c) In 3d and (d) Mo 3d for M1V-IV and reclaimed M1V-IV.

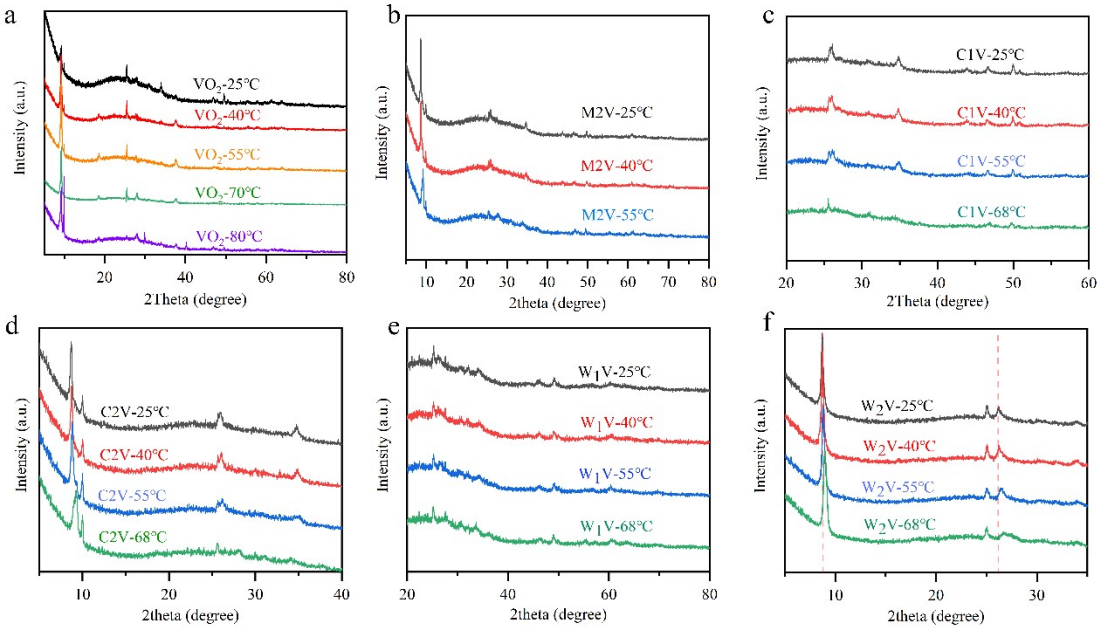

Figure S18 XRD pattern of VO_2, M2V, C1V, C2V, W1V and W2V of different temperatures.

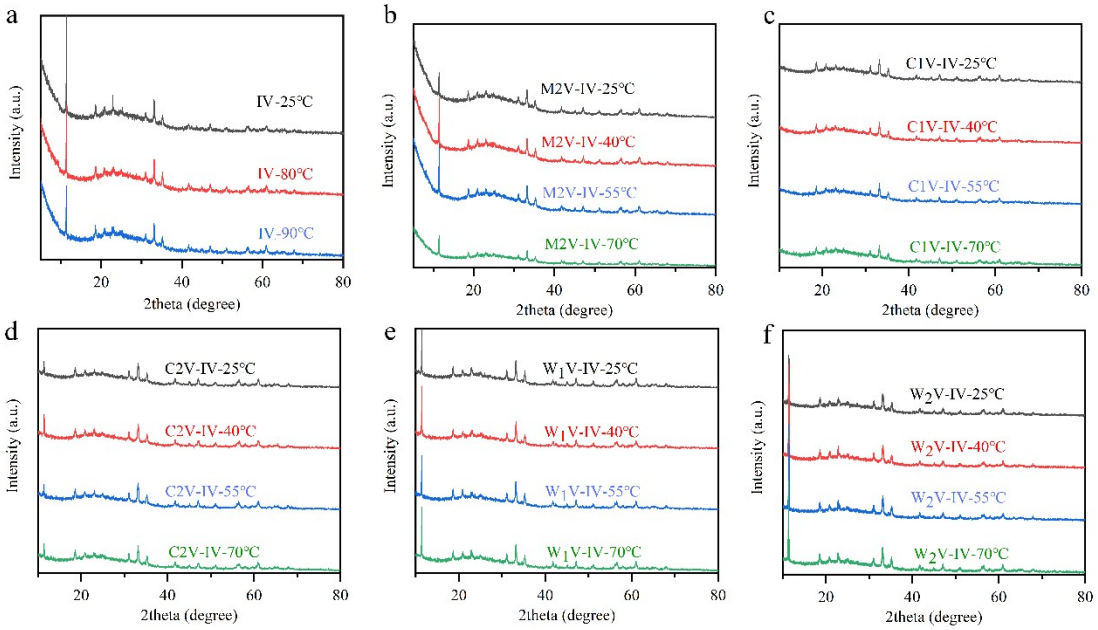

Figure S19 XRD pattern of IV, M2V-IV, C1V-IV, C2V-IV, W1V-IV and W2V-IV of different temperatures.

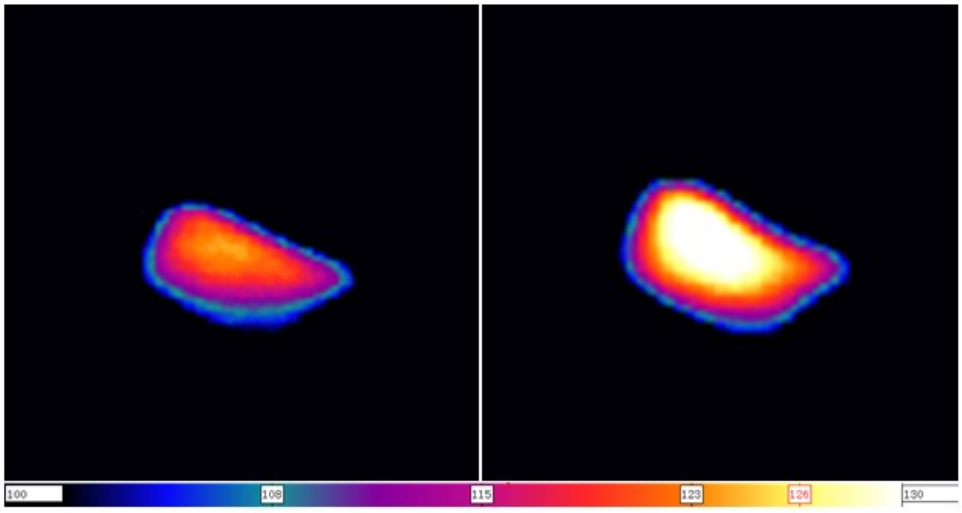

Figure S20 Infrared thermal images of VO_2-IV (left) and M1V-IV (right) for 10 min irradiation.

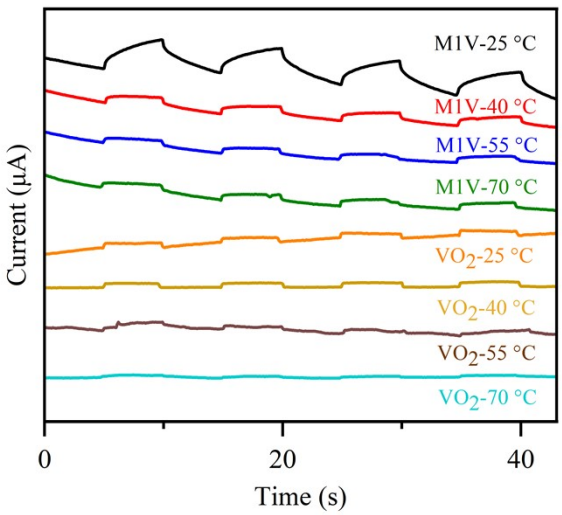

Figure S21 Transient photocurrent response with a 5 s interval of M1V and VO_2 in different temperatures

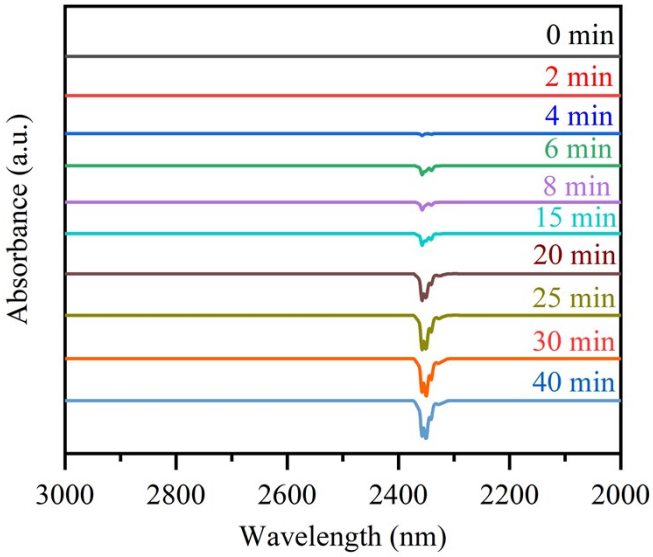

Figure S22 in situ DRIFT spectrum of M1V-IV in CO_2 atmosphere at ambient temperature in dark.

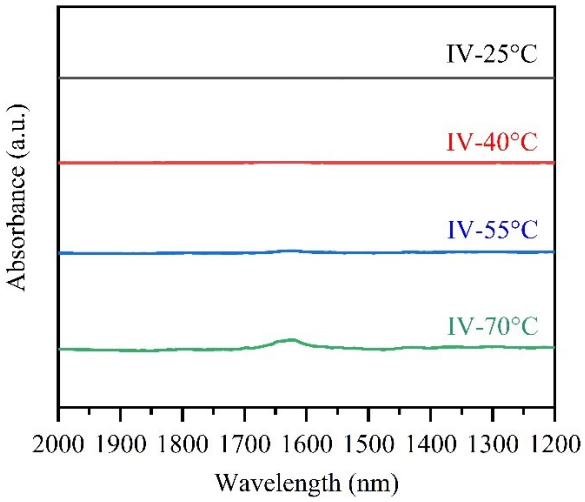

Figure S23 in situ DRIFT spectrum of IV in CO_2 atmosphere at different temperatures in dark.

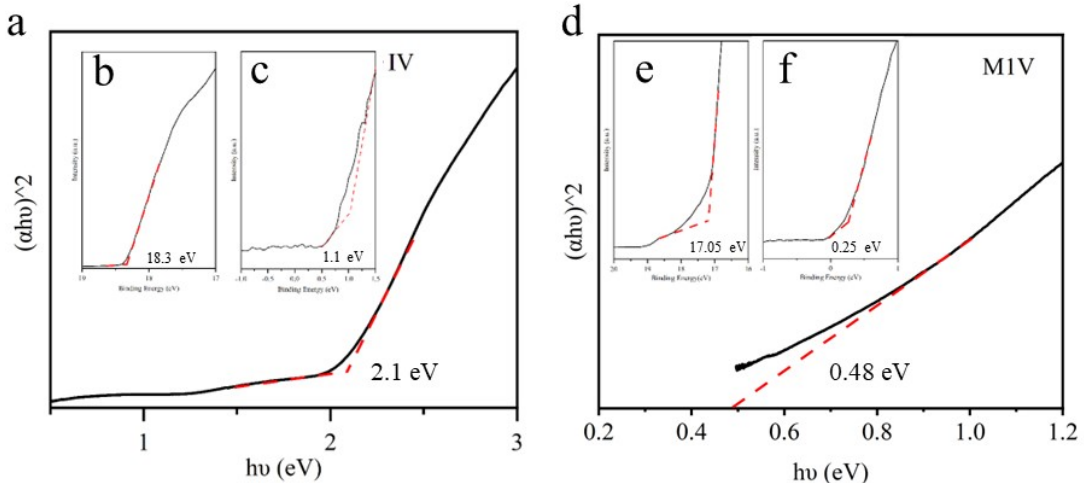

Figure S24 (a, d) Tauc plots of IV and M1V; ultraviolet photoelectron spectra (UPS) of (b, c) IV and (e, f) M1V.

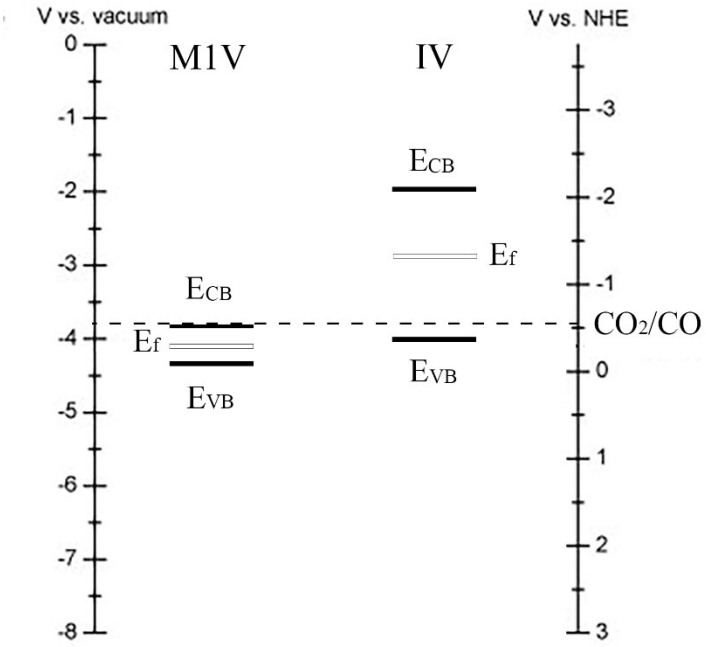

Figure S25 Position of the E_{CB} and E_{VB} for IV and M1V on the absolute vacuum energy scale and with respect to normal hydrogen electrode (NHE) (PH=7).

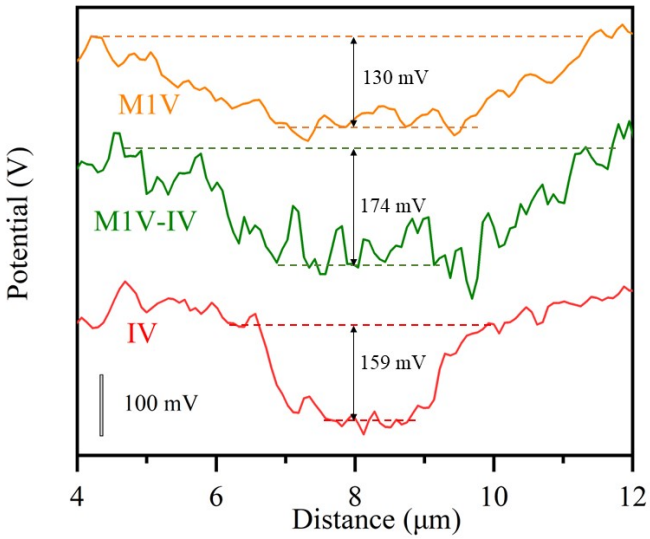

Figure S26 KPFM potential of IV, M1V and M1V-IV.

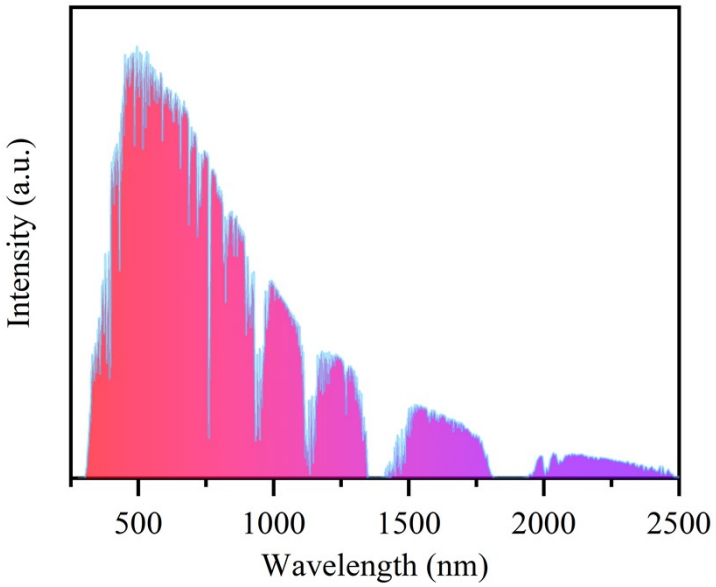

Figure S27 Simulated solar spectrogram in photocatalytic reaction.

Supplementary Table

Table S1 N_2 absorption-desorption data of different samples

Material	Single point surface area $P/P_0 = 0.27$ (m^2/g)	BET Surface Area (m^2/g)	BJH Desorption average pore diameter (nm)	Median pore width (nm)	BJH Desorption cumulative volume of pores (cm^3/g)
M1V-IV	13.9	14.0	14.34	0.746	0.067416
VO_2-IV	19.1	19.4	22.20	0.552	0.111277
M1V	7.7	7.6	23.26	0.741	0.052286
VO_2	4.6	4.5	25.43	0.554	0.016234
IV	20.9	21.3	14.75	0.752	0.091233

Table S2 the main binding energy position of samples

Sample	V 2p (eV)	O 1s	In 3d	Mo 3d/Co 2p/W 4f
IV	V^{3+} $2p_{1/2}$: 523.4 V^{3+} $2p_{5/2}$: 516.5 V^{5+} $2p_{1/2}$: 524.4 V^{5+} $2p_{3/2}$: 517.2	529.6 531.0 532.6	452.4 444.9	/
VO_2	V^{3+} $2p_{1/2}$: 522.8 V^{3+} $2p_{5/2}$: 515.1 V^{5+} $2p_{1/2}$: 524.0 V^{5+} $2p_{3/2}$: 516.4	529.1 531.5 532.8	/	/
M1V	V^{3+} $2p_{1/2}$: 523.2 V^{3+} $2p_{5/2}$: 517.7 V^{5+} $2p_{1/2}$: 524.5 V^{5+} $2p_{3/2}$: 517.1	529.7 531.4 533.0	/	234.0 230.8
M2V	V^{3+} $2p_{1/2}$: 523.1 V^{3+} $2p_{5/2}$: 515.8 V^{5+} $2p_{1/2}$: 524.5 V^{5+} $2p_{3/2}$: 523.1	529.7 531.4 533.0	/	234.0 230.8
VO_2-IV	V^{3+} $2p_{1/2}$: 523.1 V^{3+} $2p_{5/2}$: 516.2 V^{5+} $2p_{1/2}$: 524.3 V^{5+} $2p_{3/2}$: 516.8	529.4 531.0 532.5	451.6 444.1	/
M1V-IV	V^{3+} $2p_{1/2}$: 523.2 V^{3+} $2p_{5/2}$: 516.4 V^{5+} $2p_{1/2}$: 524.5 V^{5+} $2p_{3/2}$: 517.1	529.6 531.3 532.7	452.0 444.5	235.4 232.2
M2V-IV	V^{3+} $2p_{1/2}$: 523.1 V^{3+} $2p_{5/2}$: 516.4 V^{5+} $2p_{1/2}$: 524.4 V^{5+} $2p_{3/2}$: 517.0	529.7 531.3 532.8	452.0 444.5	235.4 232.2

Table S3 Comparison of products yield rates with other IV system photocatalysts.

Catalyst	Light source	Reaction condition	Productivity (μmol g^{-1} h^{-1})	Selectivity	Reference
CdSe-$InVO_4$	300 W Xe lamp visible light (λ> 420 nm)	$NaHCO_3$	CO:27.9	/	[4]
$InVO_4$-C_3N_4	Xe lamp (λ> 420 nm)	80 kPa CO_2 20 mL H_2O	CO:20.14 CH_4:3.46	85.34 %	[5]
$InVO_4$/$La_2Ti_2O_7$	300 W Xe lamp (200–780 nm, 1160 $mW.cm^{-2}$)	0.1 mL H_2O	CO:11.7	~ 100 %	[6]
C_3N_4-$InVO_4$	Xe lamp (λ> 420 nm)	5 mL H_2O	CO:14.05 CH_4:1.88	88.20 %	[7]
Bi_2WO_6/$InVO_4$	300 W Xe lamp (λ> 420 nm)	5 mL H_2O	CO:17.97 CH_4:1.12	94.11 %	[8]
BP:La/$InVO_4$:La	300 W Xe lamp (λ> 420 nm) (455 $mW.cm^{-2}$)	4 mL H_2O	CO:11.96	~ 100 %	[9]
$InVO_4$/$Ti_3C_2T_x$	300 W Xe lamp (110 $mW.cm^{-2}$)	0.4 mL H_2O	CO:13.83 CH_4:0.71	95.12 %	[10]
CdS/$InVO_4$:Eu^{3+}	300 W Xe lamp (λ> 420 nm) (455 $mW.cm^{-2}$)	4 mL H_2O	CO:11.02 CH_4:8.24	57.21 %	[11]
$InVO_4$/SiC	300 W Xe lamp visible light (λ> 420 nm)	50 μL H_2O	CO:47.53 CH_4:3.61	92.9 %	[12]
M1V-IV	300 W Xe lamp (330 $mW.cm^{-2}$)	2 mL H_2O	CO: 58 CH_4:~1	>99 %	This work

Table S4 The bi-exponential decay time constants of the time-resolved PL of samples.

Sample	τ_1/ns	A_1/%	τ_2/ns	A_2/%	τ_{ave}/ns
IV	1.00	84.19	5.52	15.81	3.31
VO_2-IV	1.70	38.22	7.24	61.78	6.54
M1V-IV	0.99	30.43	9.24	69.57	8.87

Table S5 the band position of different intermediates

Band position	Intermediates
1294	$*CO_2^-$
1395	$*COOH/CO_3^{2-}/*OCHO$
1434	$*CO_2$
1505	CO_3^{2-}
1580	*COOH
2077	CO*

Reference

[1] J.P. Perdew, K. Burke, M. Ernzerhof, Generalized Gradient Approximation Made Simple, Phys. Rev. Lett. 77, 3865 (1996)], Phys. Rev. Lett. 78 (1997) 1396.
[2] G. Kresse, and D. Joubert, From ultrasoft pseudopotentials to the projector augmented-wave method, Phys Rev B 59 (1999) 1758.
[3] P.E. Blöchl, C.J. Först, J. Schimpl, Projector augmented wave method:ab initio molecular dynamics with full wave functions, Bull. Mater. Sci. 26 (2003) 33.
[4] Feifei Mei, Kai Dai, Jinfeng Zhang, Linlin Li, Changhao Liang, Ultrathin indium vanadate/cadmium selenide-amine step-scheme heterojunction with interfacial chemical bonding for promotion of visible-light-driven carbon dioxide reduction, Journal of Colloid and Interface Science 608 (2022) 1846–1856.
[5] Mingyi Yu, Jianbo Wang, Guojun Li, Shule Zhang, Qin Zhong, Construction of 3D/2D indium vanadate/graphite carbon nitride with nitrogen defects Z-scheme heterojunction for improving photocatalytic carbon dioxide reduction, Journal of Materials Science & Technology 154 (2023) 129–139.
[6] Lujiang Xiao, Lichao Lin, Jia Song, Zizhong Zhang, Xuxu Wang, Wenyue Su, Construction of a direct Z-scheme InVO4/La2Ti2O7 photocatalyst toward efficient and selective CO2 reduction to CO, Journal of Alloys and Compounds 935 (2023) 168086.
[7] Li Wan, Deli Chen, Shuqi Miao, Fang Chen, Changfa Guo, Pengcheng Y, Jiqiang Ning, Yijun Zhong, Yong Hu, Nitric acid-assisted growth of InVO4 nanobelts on protonated ultrathin C3N4 nanosheets as an S-scheme photocatalyst with tunable oxygen vacancies for boosting CO2 conversion, Chemical Engineering Journal 434 (2022) 133867.
[8] Jiadong Li, Feng Wei, Ziyuan Xiu, Xiaojun Han, Direct Z-scheme charge transfer of Bi2WO6/InVO4 interface for efficient photocatalytic CO2 reduction, Chemical Engineering Journal 446 (2022) 137129.
[9] Qiuye Wang, Liyan Dong, Minze Li, Honglai Lu, Guodong Wei, Yang Qu, and Guofeng Wang, Z-scheme Heterojunction Photocatalyst Based on Lanthanum Single-Atom Anchored on Black Phosphorus for Regulating Surface Active Sites, therefore Enhancing Photocatalytic CO2 Reduction with ≈100% CO Selectivity, Adv. Funct. Mater. 2022, 32, 2207330.
[10] Liang Li, Yong Yang, Liuqing Yang, Xiaoyong Wang, Yong Zhou, Zhigang Zou, 3D Hydrangea-like InVO4/Ti3C2Tx Hierarchical Heterosystem Collaborating with 2D/2D Interface Interaction for Enhanced Photocatalytic CO2 Reduction, ChemNanoMat 2021, 7, 815 –823.
[11] Yini li, Yang Qu and Guofeng Wang, Europium single atom based heterojunction photocatalysts with enhanced visible-light catalytic activity, J. Mater. Chem. A, 2022, 10, 5990–5997.
[12] Hui Chen, Xin Yang, Min Lin, Dongmiao Li, Bing Wang, Jinni Shen, Jinlin Long, Wenxin Dai, Xuxu Wang, Zizhong Zhang, Dual Z‑Scheme Heterojunction SiC-Sandwiched InVO4 Nanoflowers for Boosting Visible-Light Photocatalytic CO2 Reduction with H2O, ACS Sustainable Chem. Eng. 2023, 11, 18029−18040.